ACS APPLIED MATERIALS & INTERFACES

www.acsami.org

Research Article

# Electrostatic Force-Assisted Transfer of Flexible Silicon Photodetector Focal Plane Arrays for Image Sensors

Yuting Ye,[#] Qingyan Deng,[#] Jianghong Wu, Chuyu Zhong, Hui Ma, Yilin Shi, Dingwei Li, Renjie Tang, Yiheng Tang, Jialing Jian, Bowen Zhu, Hongtao Lin, and Lan Li*

Cite This: https://doi.org/10.1021/acsami.4c05890

Read Online

ACCESS | Metrics & More | Article Recommendations | Supporting Information

**ABSTRACT:** Flexible photodetectors are pivotal in contemporary optoelectronic technology applications, such as data reception and image sensing, yet their performance and yield are often hindered by the challenge of heterogeneous integration between photoactive materials and flexible substrates. Here, we showcase the potential of an electrostatic force-assisted transfer printing technique for integrating Si PIN photodiodes onto flexible substrates. This clean and dry process eliminates the need for chemical etchants, making it a highly desirable method for manufacturing high-performance flexible photodetector arrays, expanding their widespread applications in electronic eyes, robotics, and human−machine interaction. As a demonstration, a 5 × 5 flexible Si photodetector focal plane array is constructed for imaging sensors and shaped into a convex semicylindrical form to achieve a $\pi$ field of view with long-term mechanical and thermal stability. Such an approach provides a high yield rate and consistent performance, with the single photodetector demonstrating exceptional characteristics, including a responsivity of 0.61 A/W, a response speed of 39.77 MHz, a linear dynamic range of 108.53 dB, and a specific detectivity of $2.75 \times 10^{12}$ Jones at an applied voltage of −3 V at 940 nm.

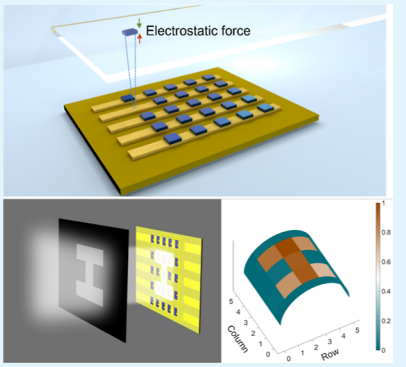


**KEYWORDS:** *si photodiode, flexible photodetector array, electrostatic force-assisted transfer, $\pi$ awareness, image sensor*



## INTRODUCTION

Flexible photodetectors with photon-to-electron conversion in the bending and stretched configuration have been widely deployed in advanced imaging systems.[1−6] However, the functionality of the flexible structures is often limited by poor device flexibility and stability; thus, the integration of photoactive materials on flexible substrates needs to be further optimized. Typically, silicon (Si) photodiodes offer the characteristics of high photosensitivity (0.59 A/W),[7] wide dynamic range (140 dB),[8] low noise current (<nA), fast dynamic response (<ns), broadband operating wavelength (400−1100 nm), and seamless integration with established Si-based complementary metal oxide semiconductor technologies,[9] demonstrating obvious advantages and potential for preparing large-scale flexible photodetector arrays. Recent advances have been made by integrating brittle Si photodiodes into precision structures with flexible substrates,[10−13] enabling the development of advanced flexible image sensors. These demonstrations involve deforming the focal plane array (FPA) using semicylindrical[14,15] and hemispherical[4,5,16] geometries, with the aim of reducing aberrations and increasing the field of view (FOV). However, a large-scale Si-based flexible photodetector array is still technically limited by efficient integration processes.

Currently, a variety of integration processes for flexible devices have been developed, including surface chemistry or adhesive-assisted transfer printing technique,[17−21] kinetically controlled transfer printing technique,[22−25] laser-driven transfer printing technique,[26−29] gecko-inspired transfer printing technique,[30−32] and aphid-inspired transfer printing technique.[33−35] These techniques have promoted the development of flexible devices, but some limitations during the integration processes still need to be optimized. For instance, transfer printing techniques that rely on surface chemistry or adhesives often result in irreversible damage to the stamp interface, limiting its reusability and leading to a degradation of device performance. While kinetically controlled transfer printing techniques offer a versatile and convenient solution, they have a limited range of adhesion regulation. Laser-driven transfer printing is a noncontact technique, but the undesirable damage to the stamp surface caused by high temperatures must be carefully considered. Consequently, there is a compelling need to develop an integration technique that is both simple to implement and compatible with various photoactive materials. This technique should also maintain the exceptional

Received: April 11, 2024
Revised: July 10, 2024
Accepted: July 11, 2024

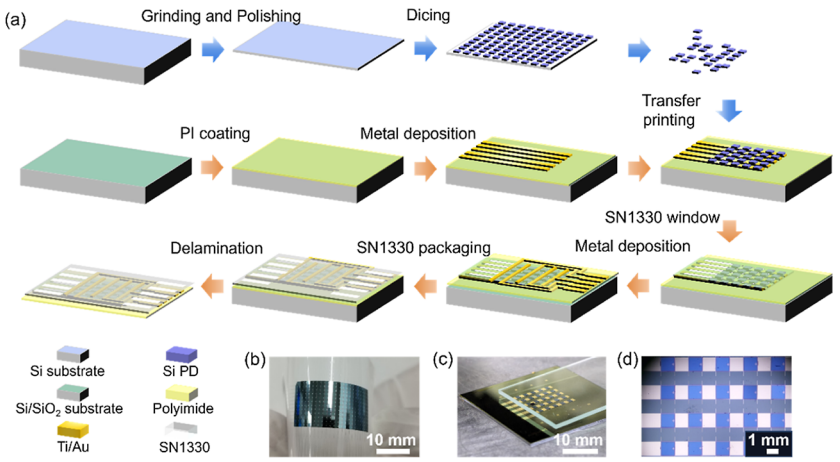


**Figure 1.** (a) Process flowchart for the preparation of flexible Si photodetector arrays; (b) Si photodiodes attached to the UV film after the dicing process; (c) electrostatic force-assisted transfer process of Si photodiodes; (d) optical microscopy image of the 5 × 5 Si photodetector array after transfer printing.

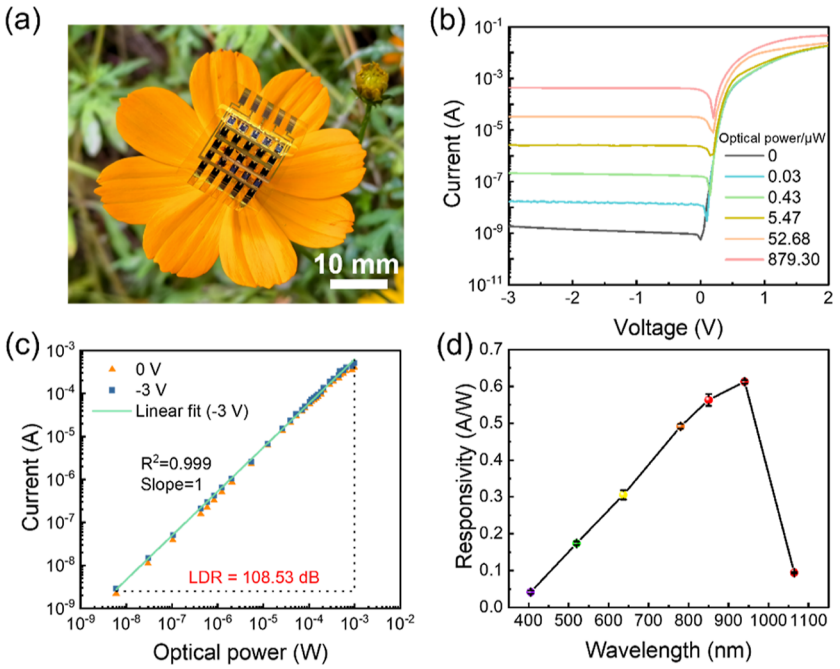


**Figure 2.** (a) Optical image of the 5 × 5 Si photodetector FPA fabricated on a polyimide substrate; (b) current−voltage ($I$−$V$) curves of a typical Si photodiode under both dark and illuminated conditions with varying optical power at 940 nm; (c) photocurrent response with respect to incident optical power at biases of −3 and 0 V, respectively; (d) spectral response of the Si photodiodes, with error bars illustrating the standard deviations from measurements on three devices.

optoelectronic properties of these materials, enabling the fabrication of high-performance photodetector FPAs on a large scale.

Here, we present an electrostatic force-assisted transfer technique to integrate semiconductor nanomembranes onto flexible substrates for image sensors. The proposed approach benefits from electrostatic adsorption to attach Si nanomembrane to a plastic slide in a dry and clean process. Taking advantage of this technique, we have demonstrated a thin-film 5 × 5 Si PIN photodetector FPA, which exhibits minimal fabrication-induced performance degradation and a 100% yield rate. The device's optoelectronic characteristics remain consistent over numerous mechanical and thermal cycles, indicating its long-term stability. Leveraging the inherent flexibility of the substrate and the absence of brittle adhesives, the FPA can be seamlessly transformed into a conformal imaging system. This system, when encapsulated, forms a compact semicylindrical imager with a radius of 3.60 mm, capable of providing a 180° in-plane FOV, a feature we refer to as "$\pi$-awareness". This conformal design enhances the system's resilience to angular variations and positions the flexible photodetector array as an effective information relay for capturing data from different spatial orientations, verified by the realized image sensor. The proposed principle and process described in this study are not limited to integrating Si photodiodes, which can be extended to other bulk materials such as GaN and InGaAs. This versatility suggests potential applications in the development of flexible multispectral imaging systems and spectrally resolved sensing devices, offering a broad impact on the field of optoelectronics.


https://doi.org/10.1021/acsami.4c05890
ACS Appl. Mater. Interfaces XXXX, XXX, XXX−XXX

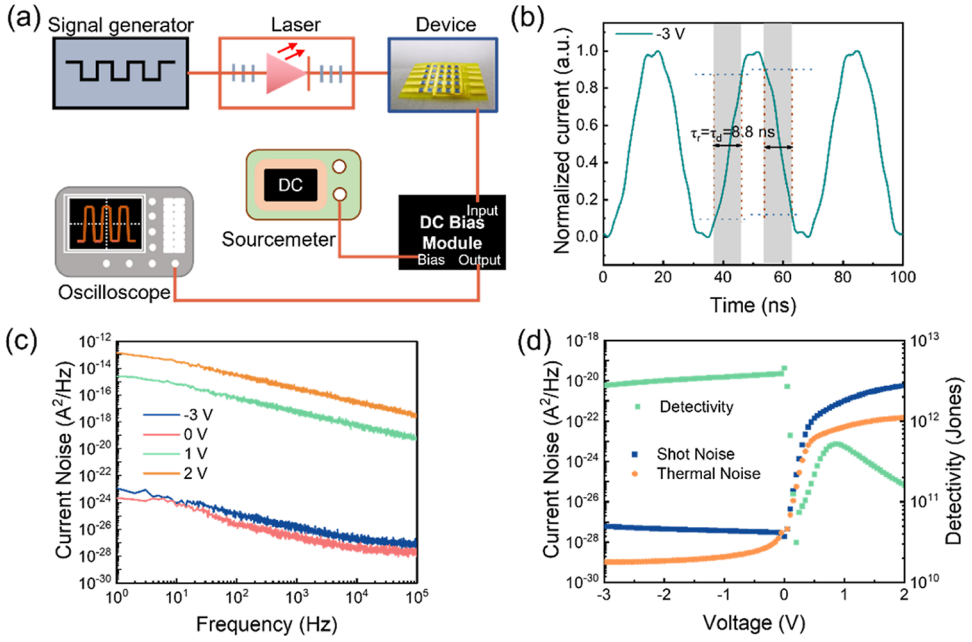


**Figure 3.** (a) Schematic setup of dynamic optoelectronic response; (b) dynamic optoelectronic response of the Si photodiode at 940 nm; (c) measured noise spectra of the Si photodetector at various applied voltages; (d) current noise and specific detectivity of the Si photodiode.

## RESULTS AND DISCUSSION

The fabrication processes are illustrated in Figure 1a, mainly including wafer grinding, Si photodiode transfer printing, and metal deposition, with further details outlined in the Methods section. As depicted in Figure 1b, the obtained photodiodes are shown affixed to a UV film after the dicing process. The integration of the photodiode onto the flexible substrate is captured in Figure 1c, illustrating the adhesion of the Si PIN photodiode onto a slide via electrostatic force. During the silicon diode transfer process, when the polystyrene slide is rubbed with dust-free paper, it becomes statically charged. This phenomenon, known as contact electrification, occurs when an originally insulating material acquires a charge through friction.[36] Electrostatic charges are generated on the surfaces of two different materials when they are brought close to each other due to differences in contact potential.[37,38] When the electrostatically charged polystyrene is brought near the silicon diode, induced charges are generated on the wafer's surface. Specifically, the surface region closest to the polystyrene develops a charge opposite to that of the polystyrene. Although the surface area further from the polystyrene also induces a charge of the same polarity, the overall effect, as described by Coulomb's law, is an attractive force between the polystyrene and the silicon diode. This integration strategy relies solely on electrostatic force without contamination or energy consumption. Lastly, during the transfer of the silicon wafer to the substrate electrode, the metallic bonding force between the materials is stronger than the electrostatic attraction between the polystyrene and the silicon wafer. This is achieved through processes such as thermal compression bonding or applying adhesives like silver paste, ensuring the successful transfer of the silicon diode to the electrode. Therefore, we develop a 5 × 5 Si photodetector array on a polyimide (PI) substrate, as illustrated in Figure 1d.

The flexible Si photodetector array is capable of conformal detection, adapting to various shapes and receiving optical signals from multiple angles, as dictated by the flexible platform's geometry, functional attributes, and light incidence properties, as depicted in Figure 2a. The optoelectronic response of a flexible Si photodiode was measured to assess its static properties. Figure 2b displays the $I-V$ curves of the photodiode for various optical powers at a wavelength of 940 nm. The observed rectification characteristic is attributed to the Si PIN junction, which yields a small dark current of 1.89 nA and an impressive current on−off ratio of $9.48 \times 10^6$ at −3 V, respectively. Additionally, a self-driven phenomenon results from the photovoltaic effect. The relationship between photocurrent and optical power over a wide optical power range is delineated in Figure 2c, demonstrating a linear correlation within the experimental limits. The linear dynamic range (LDR) is defined by LDR = 20 $\log_{10}$ ($I_{light}/I_{dark}$), where $I_{light}$ represents the photocurrent measured at a light intensity of 1 mW and $I_{dark}$ represents the dark current, yielding a large LDR of 108.53 dB. The spectral response, as shown in Figure 2d, spans from 405 to 1064 nm, with a peak responsivity ($R = I_{ph}/P_{in}$, where $I_{ph}$ and $P_{in}$ are the photocurrent and input optical power launched to the photodetector) reaching 0.61 A/W at 940 nm. The corresponding external quantum efficiency (EQE) is approximately 81%, calculated using EQE = $R_\lambda hc/q\lambda$, where $h$, $c$, $q$, and $\lambda$ represent Planck's constant, speed of light in vacuum, elementary electron charge, and the operational wavelength, respectively.

The dynamic response of the Si photodiode was assessed using a modulated laser for excitation, with the experimental setup described in Figure 3a and the Methods section. The rise and decay times of the device are both 8.80 ns (Figure 3b), and the corresponding 3 dB bandwidth is 39.77 MHz. The fast response is attributed to the vertical PIN junction structure, which enables the efficient transition and collection of photoinduced carriers driven by a built-in electric field. The total current noise in the photodetector is dominated by the $1/f$ noise, shot noise, and thermal noise. The $1/f$ noise has a spectral density of $S(f) \sim 1/f^\gamma$ (where $f$ is the frequency and $\gamma \approx 1$ is an experimental parameter)[39] and is typically present at $f$ < 100 kHz. Figure 3c displays the measured $1/f$ noise spectra


https://doi.org/10.1021/acsami.4c05890
ACS Appl. Mater. Interfaces XXXX, XXX, XXX−XXX

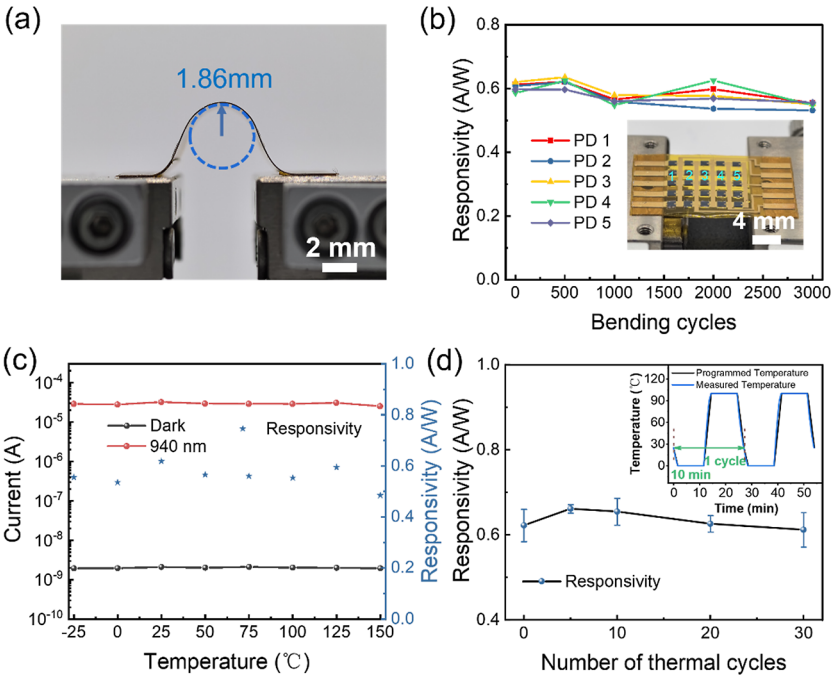


**Figure 4.** (a) Side-view photograph of the FPA bent to a radius of 1.86 mm; (b) responsivity of photodetectors at various positions after multiple bending cycles; (c) current−temperature curves (left) and responsivity-temperature (right) characteristics of the device under illumination at 940 nm; (d) responsivity of three photodetectors after various thermal cycles. Inset: The temperature profile applied during the thermal cycling tests.

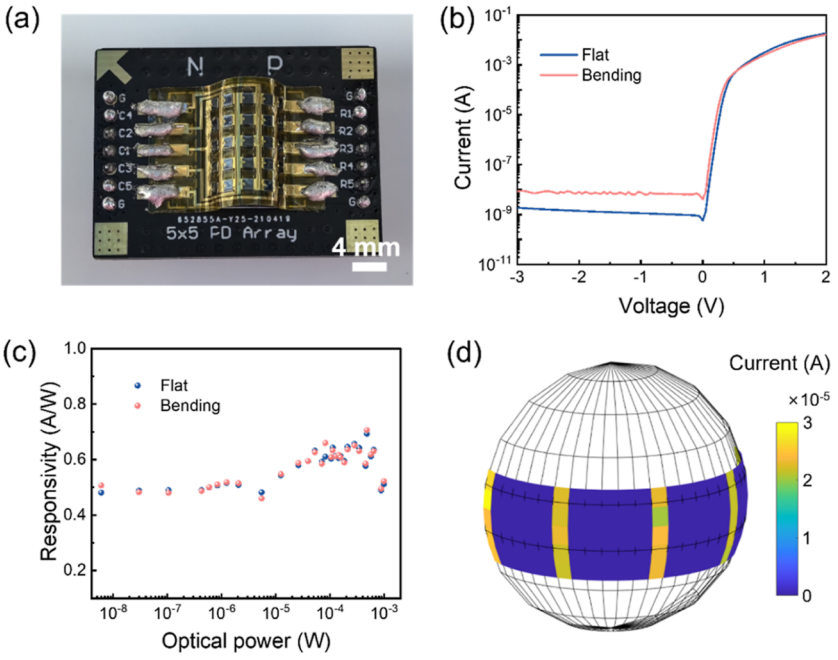


**Figure 5.** (a) Flexible FPA encapsulated on a PCB; (b) dark current and (c) responsivity of the photodetector in both planar and bent configurations; (d) photocurrent distribution map and the FOV covered by the semicylindrical FPA. Incident light power: 39.50 $\mu$W.

under different bias voltages, revealing a decrease in current noise from $1.18 \times 10^{-23}$ $A^2$/Hz at 1 Hz to $6.29 \times 10^{-28}$ $A^2$/Hz at 100 kHz under −3 V. Shot noise is the temporal fluctuation of the electric current out of equilibrium,[40] which can be expressed as $S_i = 2q \cdot i_d/\Delta f$,[41] where $i_d$ and $\Delta f$ are the dark current and bandwidth, respectively. The dark current of the photodetector is 1.89 nA at an applied voltage of −3 V, so the shot noise is $6.06 \times 10^{-28}$ $A^2$/Hz. Thermal noise, arising from the thermal fluctuations, is described by $S_t = 4k_BT/R$,[42] where $k_B$, $T$, and $R$ are the Boltzmann constant, the temperature (approximately 300 K in our experiment), and the device's resistance, respectively. The calculated thermal noise is $1.05 \times 10^{-29}$ $A^2$/Hz. Specific detectivity ($D^*$) is a crucial performance metric for evaluating photodetectors across varying active areas and operating bandwidths, since the shot noise is dominant at a high frequency here, which can be expressed by $D^* = A^{1/2} R/(2qI_d)^{1/2}$, where $A$ represents the effective area of the detector in $cm^2$ and $R$ is the responsivity in A/W. Hereby, the specific detectivity is over $2.75 \times 10^{12}$ Jones at −3 V bias (Figure 3d).


https://doi.org/10.1021/acsami.4c05890
ACS Appl. Mater. Interfaces XXXX, XXX, XXX−XXX

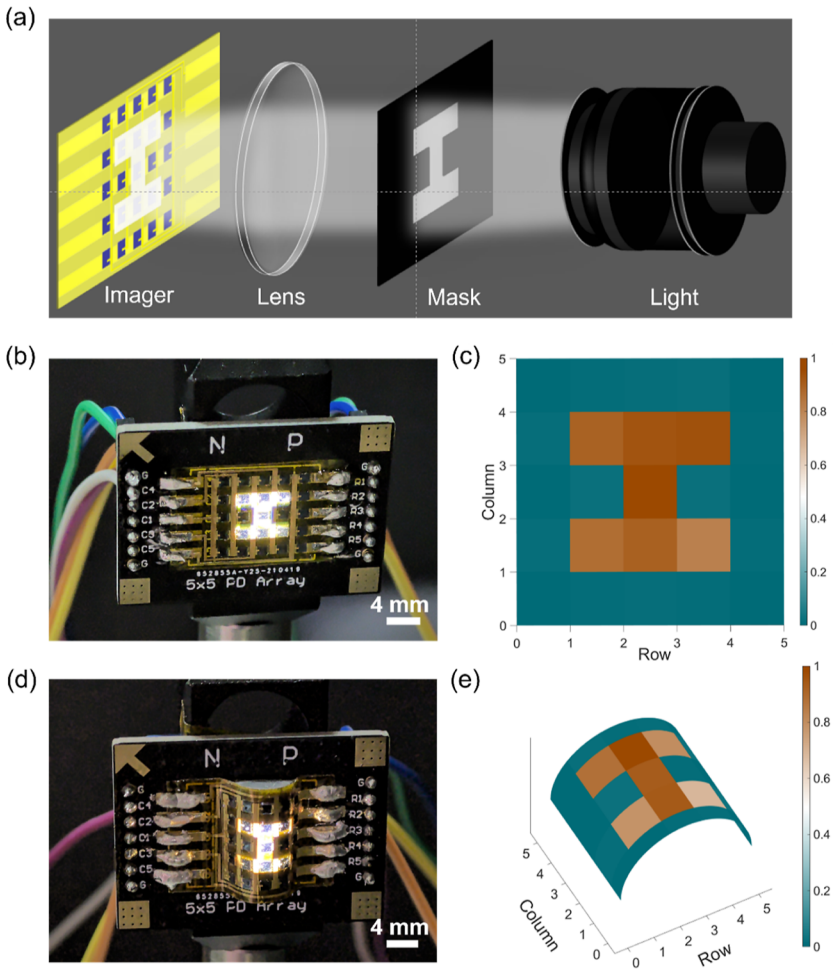


**Figure 6.** (a) Schematic diagram of the flexible image sensor's application in capturing an image of the letter *I*; (b, d) optical images formed on flat and curved imagers; (c, e) acquired current mapping of a letter *I* by the Si flexible image sensors.

The electrical and mechanical stability of flexible photodetectors under bending conditions is vital for their practical applications. The experimental setup, as illustrated in Figure 4a, involved the placement of the device on two *x*-axis displacement stages. The right stage was kept stationary, while the left stage was adjusted to induce bending with a radius of 1.86 mm. To evaluate the folding endurance, we measured dark current and photocurrent variations across five devices from the same row after subjecting them to bending cycles ranging from 0 to 3000 times. The minimal variation in responsivity (Figure 4b) attests to the devices' exceptional folding endurance. Additionally, to understand the influence of strain during bending, we conducted performance tests on the flexible detector at various bending radii (Figure S1). The data presented in Figure S2 show that the device's dark current and responsivity remained substantially stable across the different bending radii, thereby demonstrating the device's reliability and consistent performance under bending stress. Thermal stability is another crucial factor that affects the functionality of a photodetector in extreme environments. The dark current and responsivity of the device were evaluated by subjecting it to temperatures ranging from −25 to 150 °C at 25 °C intervals for 30 min. Figure 4c illustrates that the detector's performance remained stable throughout a wide temperature range. To further confirm its environmental stability, a thermal cycling test was also performed, wherein the device was subjected to 30 cycles between 0 and 100 °C, and no measurable changes in responsivity were observed (Figure 4d). Moreover, the device's high-temperature endurance was tested by exposing it to a constant 100 °C environment for 4, 8, 12, and 16 h. Even under these prolonged high-temperature conditions, the device's performance metrics remained consistent, as detailed in Figure S3. These results affirm that the realized flexible photodetector array exhibits robust mechanical and thermal stabilities, essential for their integration into flexible and portable systems.

Given the FPA's capability to be sharply curved without damage, it was wrapped into a semicylindrical shape with a 3.60 mm radius to achieve a 180° (i.e., $\pi$) FOV. To improve device integration, it was enclosed within a Printed Circuit Board (PCB) using a low-temperature solder with a melting point of 138 °C, as depicted in Figures 5a and S4. Measurements of the dark current in the device's flat state and after bending revealed a modest increase to 8.46 nA at an applied voltage of −3 V (Figure 5b). This observation may be ascribed to the multilayered structure of the flexible photodetector, where bending potentially induces alterations in the interfacial states between the constituent layers. Such interfacial modifications can modulate the recombination and transport dynamics of charge carriers, thereby resulting in an elevated dark current. However, the responsivity of the photodetector remained consistent (Figure 5c), which suggests


https://doi.org/10.1021/acsami.4c05890
ACS Appl. Mater. Interfaces XXXX, XXX, XXX−XXX

a negligible impact on the photon-to-electron conversion process. The Si photodetector FPA exhibited no significant deviation in performance when transitioned from a flat to a bent configuration, demonstrating that the mechanical strain imposed has a minimal impact on the device's functionality. This result underscores the robustness of the structural design and the dependability of the fabrication process. Based on finite element method (FEM) simulation (Figure S5), the maximal strain in all Si photodiodes is 0.32%, which is far smaller than the Si fracture limit.[43] To determine the $\pi$-object perception of the device, the fiber laser was affixed to a circular track, as illustrated in Figure S6. The photodiode array was illuminated by traversing the laser's position, halting every 36° to acquire the signal. The photocurrent signal mapping, as exhibited in Figure 5d, confirms $\pi$ awareness.

As the flexible Si photodetector FPA exhibited excellent optical sensitivity, flexibility, and stability, it was used for imaging applications, which is a pivotal component in advanced optoelectronic detection systems. Here, a prototype array with 25 pixels is applied to demonstrate the feasibility of our strategy. The experimental setup for image acquisition using light projection is presented in Figures 6a and S7, where the letter $I$ is projected onto the imager using a light source (LBTEK, LB-L21−64-WDG). Figure 6b illustrates the overall device structure of the flat flexible Si image sensor, and Figure 6c shows the resulting flat image obtained from normalized current mapping. Specifically, the normalized current, $I_{\text{normalized}}$, is based on the following equation

$$I_{\text{normalized}} = (I_{\text{light}} - I_{\text{dark}})/(I_{\text{full-light}} - I_{\text{dark}})$$

where $I_{\text{light}}$, $I_{\text{dark}}$, and $I_{\text{full-light}}$ are the measured currents under light, dark, and the full-light-illumination (all devices are exposed to light without a mask) conditions, respectively. As a comparison, the device imaging after bending is shown in Figures 6d and 6e. Crosstalk between device pixels is observed, which can be categorized into optical and electronic crosstalk. Optical crosstalk is caused by the off-axis phenomenon resulting from light diffraction, leading to interference with adjacent pixels. Electronic crosstalk, on the other hand, results from the migration of excited electrons to neighboring pixels upon exposure to incident light. As illustrated in Figure S8, a circuit analysis indicates that electrical crosstalk in our device is minimal. Consequently, the predominant source of crosstalk in the flexible image sensor is optical in nature.

## CONCLUSIONS

In summary, we have successfully demonstrated a mechanically flexible thin-film Si PIN photodetector array using the electrostatic force-assisted transfer technique. This approach brings about little contamination without additional energy consumption and ensures the fabrication of a photodetector array with excellent performance, including a responsivity of 0.61 A/W, a LDR of 108.53 dB, and a 3 dB bandwidth of 39.77 MHz. The obtained array was wrapped into semicylindrical shapes to achieve a 180° FOV and $\pi$ in-plane awareness with the suitable force arrangement. Simultaneously, the flexible photodetectors maintain stable optoelectronic performance even when subjected to bending or exposed to harsh environmental conditions. Additionally, the image sensor is demonstrated by the fabricated photodetector array. The distinctive attributes of this lightweight and flexible FPA, including its exceptional FOV, render it highly suitable for diverse applications and enable sophisticated yet streamlined optical system designs. The principle and process described in this study are not limited to the specific material systems discussed. This versatility allows for the expansion of detective materials and offers promising implications for advancing multispectral imaging and spectrally resolved sensing technologies, thereby contributing to the wider field of optoelectronics.

## METHODS

**Si Photodetector Array Fabrication.** The processes of preparing the flexible detector array started with thinning the device. Prior to this step, we commissioned a company (Innotronix Technologies Co., Ltd.) to dope the Si wafers. The wafers were thinned to approximately 50 $\mu$m using a grinding process, followed by the deposition of an electrode (comprising 5 nm Ti and 100 nm Au) on the rear surface. Subsequently, the device was mounted on a UV dicing film for scribing. Once the dicing was complete, the film was briefly exposed to UV radiation to reduce its viscosity, facilitating the separation of the detector from the film. Each detector measures approximately 1.20 mm × 1.20 mm.

A layer of the PI film was applied onto a Si wafer coated with a 500 nm layer of oxide using a spin-coating process, and a bottom metal electrode was deposited as a common anode. The photodiode was adhered to the transfer slide via electrostatic force. The Si photodiode was precisely aligned under a microscope and then transferred onto the flexible substrate. To ensure robust adhesion, a thin layer of silver paste was applied to the substrate beforehand, or the process was enhanced by metal thermal compression bonding. A layer of SN1330 photoresist (REESEEN, Jiangyin J. Wanjia Technology Co., Ltd.) was applied, with an opening for the electrode pad. A second layer of electrode (cathode) was then deposited onto the SN1330 epoxy film. The device was then encapsulated with SN1330, and photolithography was performed to define the metal electrode windows for probe contacts. Subsequently, the encapsulated device was delaminated from the substrate wafer and securely attached to commercial Kapton tape.

**Device Characterization.** The electrical characteristics were assessed through current−voltage ($I$−$V$) curve measurements utilizing a semiconductor parameter analyzer (PRIMARIUS FS-Pro). For illumination, a tunable fiber laser provides optical signals at various wavelengths. To evaluate the device's response speed, the signal generator (SIGLENT SDG6052X-E) modulates the laser to produce a square wave signal, which is then projected onto the photodiode surface. The source meter provides the bias voltage to the bias module (Thorlabs, PBM42), which connects the photodiode to the oscilloscope (SIGLENT SDS5054X). Current signals were measured using a digital source meter for the imaging and $\pi$-visual field tests (Keithley 2450).

## ASSOCIATED CONTENT

### Supporting Information

The Supporting Information is available free of charge at https://pubs.acs.org/doi/10.1021/acsami.4c05890.

Additional experimental details and methods; FEM simulation; detailed schematic and description of the experimental setup; and electrical crosstalk analysis (PDF)

## AUTHOR INFORMATION

### Corresponding Author

**Lan Li** − *Key Laboratory of 3D Micro/Nano Fabrication and Characterization of Zhejiang Province, School of Engineering, Westlake University, Hangzhou 310030, China; Institute of Advanced Technology, Westlake Institute for Advanced Study, Hangzhou 310024, China; Westlake Institute for*



https://doi.org/10.1021/acsami.4c05890
ACS Appl. Mater. Interfaces XXXX, XXX, XXX−XXX

*Optoelectronics, Fuyang, Hangzhou 311421, China;* orcid.org/0000-0002-9097-9157; Email: lilan@westlake.edu.cn

### Authors

**Yuting Ye** − *Zhejiang University, Hangzhou 310027, China; Key Laboratory of 3D Micro/Nano Fabrication and Characterization of Zhejiang Province, School of Engineering, Westlake University, Hangzhou 310030, China; Institute of Advanced Technology, Westlake Institute for Advanced Study, Hangzhou 310024, China*

**Qingyan Deng** − *Key Laboratory of 3D Micro/Nano Fabrication and Characterization of Zhejiang Province, School of Engineering, Westlake University, Hangzhou 310030, China; Institute of Advanced Technology, Westlake Institute for Advanced Study, Hangzhou 310024, China*

**Jianghong Wu** − *Key Laboratory of 3D Micro/Nano Fabrication and Characterization of Zhejiang Province, School of Engineering, Westlake University, Hangzhou 310030, China; Institute of Advanced Technology, Westlake Institute for Advanced Study, Hangzhou 310024, China*

**Chuyu Zhong** − *State Key Laboratory of Brain-Machine Intelligence, College of Information Science and Electronic Engineering, Zhejiang University, Hangzhou 310027, China*

**Hui Ma** − *State Key Laboratory of Brain-Machine Intelligence, College of Information Science and Electronic Engineering, Zhejiang University, Hangzhou 310027, China;* orcid.org/0000-0002-3670-0442

**Yilin Shi** − *Key Laboratory of 3D Micro/Nano Fabrication and Characterization of Zhejiang Province, School of Engineering, Westlake University, Hangzhou 310030, China; Institute of Advanced Technology, Westlake Institute for Advanced Study, Hangzhou 310024, China*

**Dingwei Li** − *Key Laboratory of 3D Micro/Nano Fabrication and Characterization of Zhejiang Province, School of Engineering, Westlake University, Hangzhou 310030, China; Institute of Advanced Technology, Westlake Institute for Advanced Study, Hangzhou 310024, China*

**Renjie Tang** − *Key Laboratory of 3D Micro/Nano Fabrication and Characterization of Zhejiang Province, School of Engineering, Westlake University, Hangzhou 310030, China; Institute of Advanced Technology, Westlake Institute for Advanced Study, Hangzhou 310024, China*

**Yiheng Tang** − *Key Laboratory of 3D Micro/Nano Fabrication and Characterization of Zhejiang Province, School of Engineering, Westlake University, Hangzhou 310030, China; Institute of Advanced Technology, Westlake Institute for Advanced Study, Hangzhou 310024, China*

**Jialing Jian** − *Key Laboratory of 3D Micro/Nano Fabrication and Characterization of Zhejiang Province, School of Engineering, Westlake University, Hangzhou 310030, China; Institute of Advanced Technology, Westlake Institute for Advanced Study, Hangzhou 310024, China;* orcid.org/0000-0001-6809-6588

**Bowen Zhu** − *Key Laboratory of 3D Micro/Nano Fabrication and Characterization of Zhejiang Province, School of Engineering, Westlake University, Hangzhou 310030, China; Institute of Advanced Technology, Westlake Institute for Advanced Study, Hangzhou 310024, China; Westlake Institute for Optoelectronics, Fuyang, Hangzhou 311421, China;* orcid.org/0000-0001-7534-9723

**Hongtao Lin** − *State Key Laboratory of Brain-Machine Intelligence, College of Information Science and Electronic Engineering, Zhejiang University, Hangzhou 310027, China;* orcid.org/0000-0001-7432-3644

Complete contact information is available at: https://pubs.acs.org/10.1021/acsami.4c05890

### Author Contributions

#Y.T.Y. and Q.Y.D. contributed equally to this work. Y.T.Y., L.L., and H.T.L. conceived the project. Y.T.Y., Q.Y.D., J.H.W., C.Y.Z., H.M., Y.L.S., R.J.T., and J.L.J. carried out the experiments and measurements. D.W.L., Y.H.T., and B.W.Z. analyzed the data. Y.T.Y., J.H.W., and L.L. wrote the manuscript. All authors commented on the manuscript.

### Notes

The authors declare no competing financial interest.

## ■ ACKNOWLEDGMENTS

The authors thank the Westlake Center for Micro/Nano Fabrication, Instrumentation and Service Center for Physical Sciences and Molecular Sciences at Westlake University, and ZJU Micro−Nano Fabrication Center at Zhejiang University for the facility support. This work was partially supported by the National Natural Science Foundation of China (grant nos. 12104375 and 62175202), Key R&D Program of Zhejiang Province (grant no. 2024C03150), Key Project of Westlake Institute for Optoelectronics (grant no. 2023GD003/110500Y0022303), Research Center for Industries of the Future (RCIF) at Westlake University (grant no. 210230006022302/002), and Special Support Plan for Photoelectric Chips Research at Westlake University (grant no. 10300000H062401/001).

## ■ REFERENCES

(1) Choi, C.; Leem, J.; Kim, M.; Taqieddin, A.; Cho, C.; Cho, K. W.; Lee, G. J.; Seung, H.; Bae, H. J.; Song, Y. M.; et al. Curved neuromorphic image sensor array using a $MoS_2$-organic heterostructure inspired by the human visual recognition system. *Nat. Commun.* **2020**, *11* (1), 5934.

(2) Ko, H. C.; Stoykovich, M. P.; Song, J.; Malyarchuk, V.; Choi, W. M.; Yu, C. J.; Geddes, J. B.; Xiao, J.; Wang, S.; Huang, Y.; et al. A hemispherical electronic eye camera based on compressible silicon optoelectronics. *Nature* **2008**, *454* (7205), 748−753.

(3) Jung, I.; Xiao, J.; Malyarchuk, V.; Lu, C.; Li, M.; Liu, Z.; Yoon, J.; Huang, Y.; Rogers, J. A. Dynamically tunable hemispherical electronic eye camera system with adjustable zoom capability. *Proc. Natl. Acad. Sci. U.S.A.* **2011**, *108* (5), 1788−1793.

(4) Song, Y. M.; Xie, Y.; Malyarchuk, V.; Xiao, J.; Jung, I.; Choi, K.-J.; Liu, Z.; Park, H.; Lu, C.; Kim, R.-H.; et al. Digital cameras with designs inspired by the arthropod eye. *Nature* **2013**, *497* (7447), 95−99.

(5) Zhang, K.; Jung, Y. H.; Mikael, S.; Seo, J.-H.; Kim, M.; Mi, H.; Zhou, H.; Xia, Z.; Zhou, W.; Gong, S.; et al. Origami silicon optoelectronics for hemispherical electronic eye systems. *Nat. Commun.* **2017**, *8* (1), 1782.

(6) Rao, Z.; Lu, Y.; Li, Z.; Sim, K.; Ma, Z.; Xiao, J.; Yu, C. Curvy, shape-adaptive imagers based on printed optoelectronic pixels with a kirigami design. *Nat. Electron.* **2021**, *4*, 513−521.

(7) Kim, K.; Yoon, S.; Seo, M.; Lee, S.; Cho, H.; Meyyappan, M.; Baek, C.-K. Whispering gallery modes enhance the near-infrared photoresponse of hourglass-shaped silicon nanowire photodiodes. *Nat. Electron.* **2019**, *2* (12), 572−579.

(8) Garcia, M.; Davis, T.; Blair, S.; Cui, N.; Gruev, V. Bioinspired polarization imager with high dynamic range. *Optica* **2018**, *5* (10), 1240−1246.

(9) Chou, F.-P.; Chen, G.-Y.; Wang, C.-W.; Liu, Y.-C.; Huang, W.-K.; Hsin, Y.-M. Silicon photodiodes in standard CMOS technology. *IEEE J. Sel. Top. Quantum Electron.* **2011**, *17* (3), 730−740.
(10) Sun, Y.; Rogers, J. A. Inorganic semiconductors for flexible electronics. *Adv. Mater.* **2007**, *19* (15), 1897−1916.
(11) Park, S.-I.; Xiong, Y.; Kim, R.-H.; Elvikis, P.; Meitl, M.; Kim, D.-H.; Wu, J.; Yoon, J.; Yu, C.-J.; Liu, Z.; et al. Printed assemblies of inorganic light-emitting diodes for deformable and semitransparent displays. *Science* **2009**, *325* (5943), 977−981.
(12) Yu, K. J.; Yan, Z.; Han, M.; Rogers, J. A. Inorganic semiconducting materials for flexible and stretchable electronics. *npj Flexible Electron.* **2017**, *1* (1), 4.
(13) Chen, Y.; Zhang, Y.; Liang, Z.; Cao, Y.; Han, Z.; Feng, X. Flexible inorganic bioelectronics. *npj Flexible Electron.* **2020**, *4* (1), 2.
(14) Floreano, D.; Pericet-Camara, R.; Viollet, S.; Ruffier, F.; Brückner, A.; Leitel, R.; Buss, W.; Menouni, M.; Expert, F.; Juston, R.; et al. Miniature curved artificial compound eyes. *Proc. Natl. Acad. Sci. U.S.A.* **2013**, *110* (23), 9267−9272.
(15) Viollet, S.; Godiot, S.; Leitel, R.; Buss, W.; Breugnon, P.; Menouni, M.; Juston, R.; Expert, F.; Colonnier, F.; L'Eplattenier, G.; et al. Hardware architecture and cutting-edge assembly process of a tiny curved compound eye. *Sensors* **2014**, *14* (11), 21702−21721.
(16) Rao, Z.; Lu, Y.; Li, Z.; Sim, K.; Ma, Z.; Xiao, J.; Yu, C. Curvy, shape-adaptive imagers based on printed optoelectronic pixels with a kirigami design. *Nat. Electron.* **2021**, *4* (7), 513−521.
(17) Ahn, J.-H.; Kim, H.-S.; Lee, K. J.; Jeon, S.; Kang, S. J.; Sun, Y.; Nuzzo, R. G.; Rogers, J. A. Heterogeneous three-dimensional electronics by use of printed semiconductor nanomaterials. *Science* **2006**, *314* (5806), 1754−1757.
(18) Baca, A. J.; Meitl, M. A.; Ko, H. C.; Mack, S.; Kim, H. S.; Dong, J.; Ferreira, P. M.; Rogers, J. A. Printable single-crystal silicon micro/nanoscale ribbons, platelets and bars generated from bulk wafers. *Adv. Funct. Mater.* **2007**, *17* (16), 3051−3062.
(19) Lee, C. H.; Kim, D. R.; Zheng, X. Fabricating nanowire devices on diverse substrates by simple transfer-printing methods. *Proc. Natl. Acad. Sci. U.S.A.* **2010**, *107* (22), 9950−9955.
(20) Kim, T.-i.; Kim, M. J.; Jung, Y. H.; Jang, H.; Dagdeviren, C.; Pao, H. A.; Cho, S. J.; Carlson, A.; Yu, K. J.; Ameen, A.; et al. Thin film receiver materials for deterministic assembly by transfer printing. *Chem. Mater.* **2014**, *26* (11), 3502−3507.
(21) Choi, M. K.; Yang, J.; Kang, K.; Kim, D. C.; Choi, C.; Park, C.; Kim, S. J.; Chae, S. I.; Kim, T.-H.; Kim, J. H.; et al. Wearable red-green-blue quantum dot light-emitting diode array using high-resolution intaglio transfer printing. *Nat. Commun.* **2015**, *6* (1), 7149.
(22) Meitl, M. A.; Zhu, Z.-T.; Kumar, V.; Lee, K. J.; Feng, X.; Huang, Y. Y.; Adesida, I.; Nuzzo, R. G.; Rogers, J. A. Transfer printing by kinetic control of adhesion to an elastomeric stamp. *Nat. Mater.* **2006**, *5* (1), 33−38.
(23) Cho, S.; Kim, N.; Song, K.; Lee, J. Adhesiveless transfer printing of ultrathin microscale semiconductor materials by controlling the bending radius of an elastomeric stamp. *Langmuir* **2016**, *32* (31), 7951−7957.
(24) Chen, H.; Feng, X.; Chen, Y. Directionally controlled transfer printing using micropatterned stamps. *Appl. Phys. Lett.* **2013**, *103* (15), 151607.
(25) Yoon, J.; Jo, S.; Chun, I. S.; Jung, I.; Kim, H.-S.; Meitl, M.; Menard, E.; Li, X.; Coleman, J. J.; Paik, U.; et al. GaAs photovoltaics and optoelectronics using releasable multilayer epitaxial assemblies. *Nature* **2010**, *465* (7296), 329−333.
(26) Chen, F.; Gai, M.; Sun, N.; Xu, Z.; Liu, L.; Yu, H.; Bian, J.; Huang, Y. Laser-driven hierarchical "gas-needles" for programmable and high-precision proximity transfer printing of microchips. *Sci. Adv.* **2023**, *9* (43), No. eadk0244.
(27) Wang, C.; Linghu, C.; Nie, S.; Li, C.; Lei, Q.; Tao, X.; Zeng, Y.; Du, Y.; Zhang, S.; Yu, K.; et al. Programmable and scalable transfer printing with high reliability and efficiency for flexible inorganic electronics. *Sci. Adv.* **2020**, *6* (25), No. eabb2393.
(28) Saeidpourazar, R.; Li, R.; Li, Y.; Sangid, M. D.; Lu, C.; Huang, Y.; Rogers, J. A.; Ferreira, P. M. Laser-driven micro transfer placement of prefabricated microstructures. *J. Microelectromech. Syst.* **2012**, *21* (5), 1049−1058.
(29) Gao, Y.; Li, Y.; Li, R.; Song, J. An accurate thermomechanical model for laser-driven microtransfer printing. *J. Appl. Mech.* **2017**, *84* (6), 064501.
(30) Yoo, B.; Cho, S.; Seo, S.; Lee, J. Elastomeric angled microflaps with reversible adhesion for transfer-printing semiconductor membranes onto dry surfaces. *ACS Appl. Mater. Interfaces* **2014**, *6* (21), 19247−19253.
(31) Mengüç, Y.; Yang, S. Y.; Kim, S.; Rogers, J. A.; Sitti, M. Gecko-inspired controllable adhesive structures applied to micromanipulation. *Adv. Funct. Mater.* **2012**, *22* (6), 1246−1254.
(32) Jeong, J.; Kim, J.; Song, K.; Autumn, K.; Lee, J. Geckoprinting: assembly of microelectronic devices on unconventional surfaces by transfer printing with isolated gecko setal arrays. *J. R. Soc., Interface* **2014**, *11* (99), 20140627.
(33) Linghu, C.; Wang, C.; Cen, N.; Wu, J.; Lai, Z.; Song, J. Rapidly tunable and highly reversible bio-inspired dry adhesion for transfer printing in air and a vacuum. *Soft Matter* **2019**, *15* (1), 30−37.
(34) Li, Y.; Zhang, F.; Wang, S. Regulatable interfacial adhesion between stamp and ink for transfer printing. *Interdiscip. Mater.* **2024**, *3* (1), 29−53.
(35) Carlson, A.; Wang, S.; Elvikis, P.; Ferreira, P. M.; Huang, Y.; Rogers, J. A. Active, programmable elastomeric surfaces with tunable adhesion for deterministic assembly by transfer printing. *Adv. Funct. Mater.* **2012**, *22* (21), 4476−4484.
(36) Lacks, D. J.; Sankaran, R. M. Contact electrification of insulating materials. *J. Phys. D: Appl. Phys.* **2011**, *44* (45), 453001.
(37) Yan, Y.; Hu, Y.; Wang, L.; Qian, X.; Zhang, W.; Reda, K.; Wu, J.; Zheng, G. Electrostatic sensors-Their principles and applications. *Measurement* **2021**, *169*, 108506.
(38) Chen, L.; Shi, Q.; Sun, Y.; Nguyen, T.; Lee, C.; Soh, S. Controlling surface charge generated by contact electrification: strategies and applications. *Adv. Mater.* **2018**, *30* (47), 1802405.
(39) Johnson, J. B. The Schottky effect in low frequency circuits. *Phys. Rev.* **1925**, *26* (1), 71−85.
(40) Blanter, Y. M.; Büttiker, M. Shot noise in mesoscopic conductors. *Phys. Rep.* **2000**, *336* (1−2), 1−166.
(41) Li, L.; Lin, H.; Huang, Y.; Shiue, R.; Yadav, A.; Li, J.; Michon, J.; Englund, D.; Richardson, K.; Gu, T.; Hu, J. High-performance flexible waveguide-integrated photodetectors. *Optica* **2018**, *5* (1), 44.
(42) Wu, J.; Wei, M.; Mu, J.; Ma, H.; Zhong, C.; Ye, Y.; Sun, C.; Tang, B.; Wang, L.; Li, J.; et al. High-performance waveguide-integrated $Bi_2O_2Se$ photodetector for Si photonic integrated circuits. *ACS Nano* **2021**, *15* (10), 15982−15991.
(43) Chen, M.; Pethö, L.; Sologubenko, A. S.; Ma, H.; Michler, J.; Spolenak, R.; Wheeler, J. M. Achieving micron-scale plasticity and theoretical strength in Silicon. *Nat. Commun.* **2020**, *11* (1), 2681.


https://doi.org/10.1021/acsami.4c05890
*ACS Appl. Mater. Interfaces* XXXX, XXX, XXX−XXX